
Universiteit
Leiden
The Netherlands

Millimeter emission from protoplanetary disks : dust, cold gas, and relativistic electrons

Salter, D.M.

Citation
Salter, D. M. (2010, November 25). *Millimeter emission from protoplanetary disks : dust, cold gas, and relativistic electrons*. Leiden Observatory, Faculty of Science, Leiden University. Retrieved from https://hdl.handle.net/1887/16175

Version:	Corrected Publisher's Version
License:	Licence agreement concerning inclusion of doctoral thesis in the Institutional Repository of the University of Leiden
Downloaded from:	https://hdl.handle.net/1887/16175

Note: To cite this publication please use the final published version (if applicable).

Table 3.3 — CO spectra statistics.

Source	CO Trans.	v_{LSR} [km s^{-1}]	σ_{rms} [mJy bm^{-1}]	I_{max} [mJy bm^{-1}]	S/N	I_{peak} [mJy bm^{-1}]	FWHM [km s^{-1}]	$\int I\,dv$ [mJy bm$^{-1}\cdot$ km s^{-1}]
CW Tau	1–0	-	16.0	-	-	-	1.0	$\leq$31.5
DQ Tau	1–0	-	11.4	-	-	-	1.0	$\leq$22.5
	2–1	10.5	6.6	38.3	5.8	38.6	0.5	48.3
IQ Tau	1–0	-	12.1	-	-	-	1.0	$\leq$20.9
V806 Tau	1–0	5.2	11.0	60.5	5.5	53.9	1.2	67.6
	1–0	1.1	11.0	46.7	4.2	45.6	1.0	57.2
	1–0	12.2	11.0	23.4	2.1	35.4	0.4	44.4
V892 Tau	1–0	5.4	26.6	88.2	3.3	82.2	0.9	90.9
	1–0	0.5	26.6	89.3	3.4	98.8	0.5	68.2
	1–0	12.7	26.6	90.7	3.4	76.6	0.9	91.5

Notes. For each source, we give the central radio velocity v_{LSR} for each emission line detected, the noise level σ_{rms} for the spectrum, the maximum intensity I_{max} value in the binned data set, the signal-to-noise ratio, the peak intensity I_{peak} from a Gaussian fit to the line, the FWHM of each line, and the integrated line intensity. For non-detections, we report only a 3σ upper limit where $\sigma = 1.2\sigma_{rms}\sqrt{\Delta V\,\delta v}$ following Jørgensen et al. (2004).

Table 3.4 — Disk parameters.

	DUST					*GAS*					
Source	u,v Range [kλ]	Size [$''$]	Size [AU]	i [$^\circ$]	PA [$^\circ$]	Line	u,v Range [kλ]	Size [$''$]	Size [AU]	i [$^\circ$]	PA [$^\circ$]
CW Tau	(0,200)	0.57×0.32	80×45	56	42.4	(1–0)	···	···	···	···	···
DQ Tau	(0,200)	0.40×0.37	56×52	22	42.4	(2–1)	(0,80)	1.86×0.87	260×122	62	27.8
IQ Tau	(0,200)	0.56×0.55	78×77	11	80.0	(1–0)	···	···	···	···	···
V806 Tau	(0,70)	1.22×0.81	171×113	48	-75.2	(1–0)	(0,70)	3.68×2.37	515×332	50	-77.2
V892 Tau	(0,40)	2.30×1.22	322×171	58	-62.9	(1–0)	(0,40)	4.90×0.56	686×78	83	28.7
$''$	(40,200)	0.4×0.3	56×36	49	48.7	(1–0)	(40,200)	0.25×0.21	35×29	33	-84.9

Notes. Results of a Gaussian fit to each visibility data set, using the Miriad *uvfit* routine. In the leftmost columns, the derived values are for the continuum (dust) data, and on the right the results are for the spectral line (CO) data. We also indicate the u,v range used where the signal-to-noise was reliable for a good fit.

studies of the system that find a value of 157° (Boden et al. 2009). The projection of the gas disk on the sky appears flatter, suggesting a larger inclination value of 62°. The CO flux returned by the fit is 0.4 Jy.

We also determine that a similarly bright line at the 1–0 frequency may not have been detected in our CARMA observations, peaking instead at about 1.6σ, which is not unlike the noise peak seen in the DQ Tau spectrum at the source radial velocity, determined to be $10.6\,\mathrm{km\,s^{-1}}$ from the 2–1 data (Table 3.3). However, as we determined in Section 3.3.2, the noise peak in the 1–0 data does not originate from the source position. Finally, as a sanity check due to the unusual flare activity observed in the 3 mm continuum band toward DQ Tau on 2008 April 19, we can confirm that the CO (1–0) line remained undetected on the flare date as on the quiescent dates. Therefore, no unexpected behavior is likely (or has been observed) to affect the CO (2–1) detection despite it being observed during a subsequent brightening (as seen at longer wavelengths).

3.4.3 V806 Tau

V806 Tau (also known as Haro 6-13) is the second brightest source in our sample at 2.7 mm, and it is one of only two sources to be resolved in the continuum. Our visibility data seems best approximated by a single structure. We extrapolate from the visibility amplitudes that the source becomes resolved near $100\,\mathrm{k}\lambda$, which corresponds to an angular size of $2.5''$ on the sky. At the distance to Taurus, we estimate that the emission originates in a dust disk of radius 175 AU. This is consistent with the fit found by the Miriad *uvfit* routine, which we provide in Table 3.4.

In the CO (1–0) spectra toward V806 Tau, two strong peaks are detected at radial velocities of 1.1 and $5.2\,\mathrm{km\,s^{-1}}$ (as listed in Table 3.3). The CO emission contributing to both peaks coincides with the source position, as can be seen in the CO maps in Figure 3.4. There we show the integrated intensity maps for an $\sim 1\,\mathrm{km\,s^{-1}}$ wide velocity bin centered around each of the *three* brightest features in the spectra. The third tentative ($\sim 2.9\sigma$) spectal peak at $12\,\mathrm{km\,s^{-1}}$ is related to emission located away from the source position and is likely noise. In the other two bins, the CO distribution measures just 4σ above the sky levels and appears clumpy. At the source radial velocity, presumed to be the central velocity of the brightest peak ($v = 5.2\,\mathrm{km\,s^{-1}}$), the emission is concentrated at the dust continuum peak. In the blueshifted velocity bin near $1.1\,\mathrm{km\,s^{-1}}$, the emission appears as an arc about one side of the continuum source position. It is therefore interesting to return to the redshifted emission map where the prominent (and extended) noise peak lies opposite the blueshifted emission at roughly an equal radial distance from the location of the continuum peak. The velocities of the two bins are also rather symmetric about the central source velocity ($\Delta v \approx \pm 5.5\,\mathrm{km\,s^{-1}}$), leading us to ask whether the CO emission presents a much broader line profile and only these three peaks sit above the noise levels, since emission at these velocity offsets (Δv) can be attributed to gas at a radial distance of ≤ 29 AU from a $1\,M_{\odot}$ central star.

We recall that V806 Tau is the only source to be resolved in the CO (1–0) emission. The visibility data for the emission at the source velocity, as plotted in column 3 of Figure 3.2, detects structure out to $40\,\mathrm{k}\lambda$. Performing a Gaussian fit to the visibility amplitudes for the central line only ($v = 5.2\,\mathrm{km\,s^{-1}}$), we derive a gas disk of size 515×332 AU. The disk inclination from this fit is identical to the inclination determined from the dust, providing support for a similar (gas and dust) disk structure. The derived gas extent is consistent with the $6''$ angular separation between the redshifted "noise" peak and the blueshifted CO peak, even though these channels were not included in the fit. It is still unclear, however, why the highest shifted velocities would be located at the largest disk radii. One explanation might be that a majority of the CO is obscured by intervening cloud material and the emission at these radial velocities and locations are the least affected.

Recently, Schaefer et al. (2009) also presented 3 mm-band data of V806 Tau using the IRAM PdBI. With a higher spectral resolution and sensitivity, they are able to document significant cloud contamination at the central source velocity, confirming obscuration of the line. In general, the rest of our results

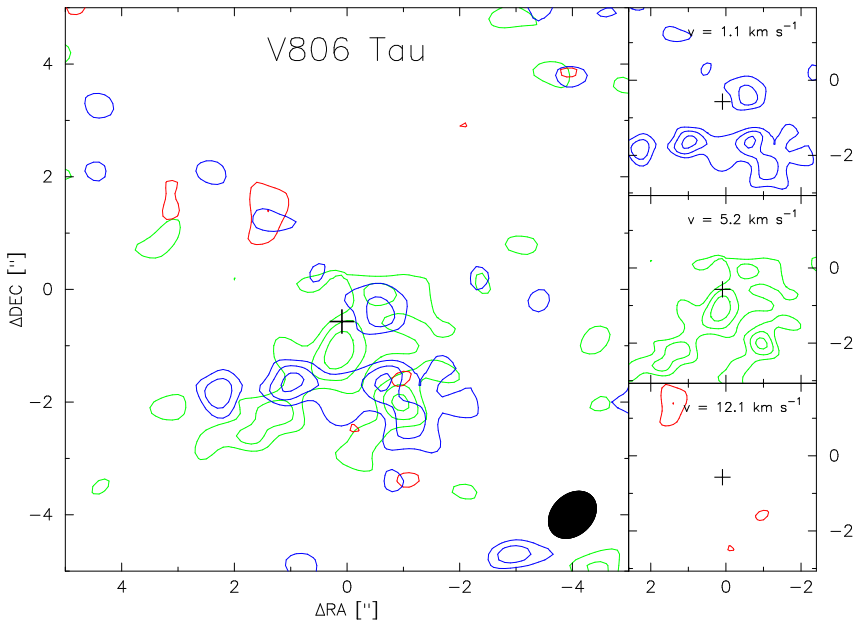

Figure 3.4 — The CO moment 0 maps for V806 Tau. Contours are drawn at 2, 3, and 4σ where σ is 4.7 Jy bm^{-1}· km s^{-1} in all panels. The large panel at left is a $10'' \times 10''$ composite map overlaying the three velocity ranges corresponding to the brightest peaks in the spectra in Figure 3.2. On the right, the three separate maps are shown in the $5'' \times 5''$ integration box used to create the spectra. The central velocity for each map is given in the upper right-hand corner and the statistical details are provided in Table 3.3. Crosses indicate the location of the dust continuum peak.

are consistent. They report a continuum flux of 29.5 ± 0.6 mJy at 2.6 mm versus our 35.7 mJy, which is well within typical flux calibration errors. They cover a velocity range of 1.9–8.7 km s^{-1}, and find evidence of extended emission and high-velocity wings, which they attribute instead to a possible outflow. Their maps do not cover the velocity range of our blueshifted peak. However, in CSO single-dish observations of the ^{12}CO (3–2) line towards this source, Moriarty-Schieven et al. (1992) report no evidence for outflows (defined in their sample as wing breadths $\Delta v > 6$ km s^{-1}); but they do find evidence for extended cloud emission in a velocity range of 7–11 km s^{-1}, which may explain the lack of redshifted emission in our own interferometry data. Schaefer et al. (2009) find an inclination of 40° (compared to our 50°) and an outer gas radius > 180 AU (consistent with our projected size of 515×332 AU) from a detailed kinematical study of the CO emission that is hindered greatly by obscuration of the line in the outer channel data as well, and indicating that the obscuration is not limited to a small velocity range.

3.4.4 V892 Tau

The V892 Tau (also known as Haro 6-5) spectrum exhibits two emission peaks with a wide velocity separation (at 5.4 and 12.7 km s^{-1}). We also notice that the blueshifted end of the spectrum appears "noisier". However, an inspection of the inidvidual channel maps suggests that these channels contain low-level (2–3σ) emission originating from near the continuum dust position that may be real. As an example, we include in Figure 3.5 a moment 0 map for the velocity bin at 0.5 km s^{-1} (width $\sim$1 km s^{-1}) when we analyze the spatial distribution of the spectral line emission peaks.

In the literature, there is evidence for outflows and intervening cloud material along the line-of-sight toward this source. Thi et al. (2001) observed V892 Tau with the JCMT single-dish telescope in the CO (3–2) line and report a broad spectrum (spanning ≈ 6 km s^{-1}) with bright emission, but that emission only possesses radial velocities between our CARMA central (5.4 km s^{-1}) and redshifted (12.7 km s^{-1})

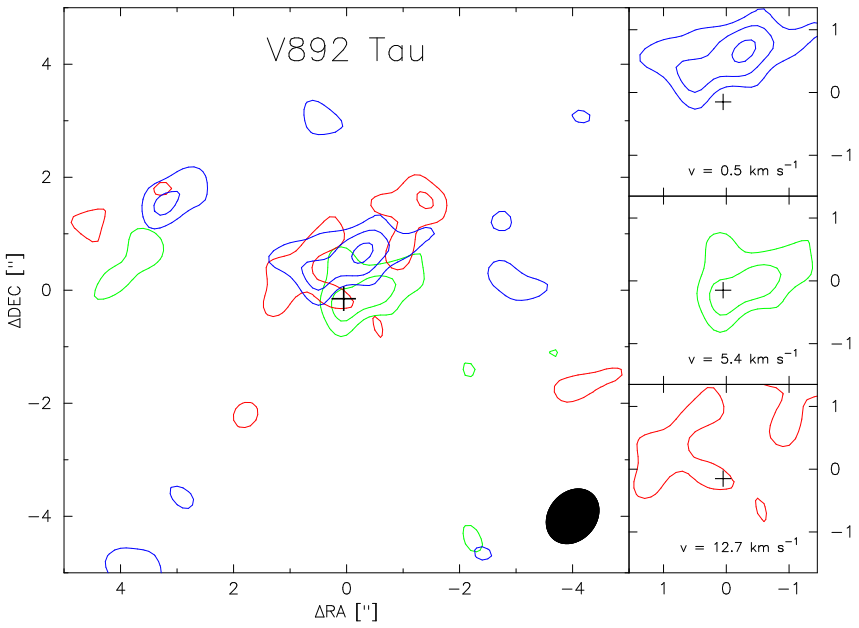

Figure 3.5 — CO moment 0 maps of V892 Tau. Contours are drawn at 2, 3, and 4σ where σ is 5.5 Jy bm^{-1} km s^{-1}. Identical to Figure 3.4, except that the individual maps are shown in a $3'' \times 3''$ integration box used for the spectra in Figure 3.2.

peaks (see Figure 3.6). In contrast, the complementary (6–5) line observed by Thi et al. (2001) has a strong peak centered at 8.8 km s^{-1} accompanied by a noisy wing extending bluewards until a velocity of about 5.5 km s^{-1}. Given our CARMA (1–0) results, we might also be tempted to identify an isolated redshifted peak near 13 km s^{-1} in the 6–5 data.

A broader line is to be expected from a more massive central star (5.5 $M_{\odot}$) with a B8 V spectral type (Monnier et al. 2008), especially at a high inclination. However, mapping of a $90'' \times 90''$ region around V892 Tau with the HARP-B receiver on the JCMT reveals a very similar, broad emission profile at 11 separate off-source positions (see Panić & Hogerheijde 2009). Likewise, we attribute the fact that we do not see bright CO (1–0) emission from such a bright source in the interferometry data to resolved-out, large-scale, optically thick emission over the same velocity range. To better probe the gas content in this disk, it will be necessary to consider optically thinner molecular tracers to better contrast the contribution from the disk versus the surrounding cloud material.

In the continuum, the source is found by dust continuum analyses in the literature to have an inclination of 60° (Hamidouche 2010; Monnier et al. 2008), which is consistent with a double-peaked line as seen clearly in the CO (3–2) and (6–5) data (see Figure 3.6, reproduced from Thi et al. 2001). We report a similar inclination (58°) based on a simple Gaussian fit to our continuum (dust) visibility data and using an analysis of the aspect ratio to derive the source size.

3.5 Discussion

Our gas-line properties (e.g. line intensities and spatial extent) are not always in agreement with predictions made based on the dust properties of each source. For example, our brightest continuum source V892 Tau is only detected weakly in CO (1–0), whereas our second brightest source V806 Tau, at half the flux of V892 Tau, exhibits a strong integrated spectral line and a spatially extended gas reservoir. Along these same lines, DQ Tau and IQ Tau are two equally bright sources in the continuum, both undetected in 1–0, but DQ Tau appears very bright in 2–1 while IQ Tau remains undetected (see Schaefer et al. 2009).

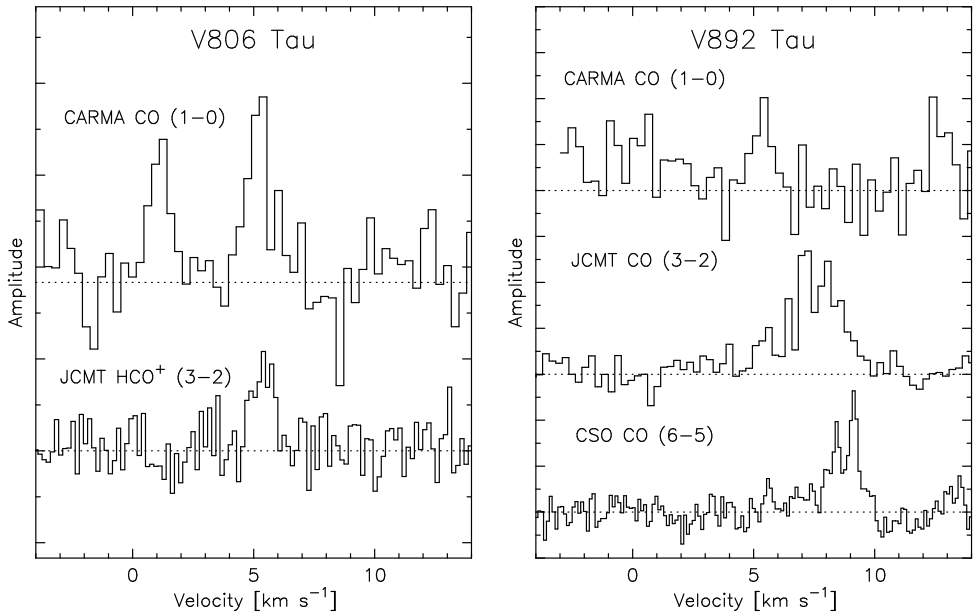

Figure 3.6 — A comparison of our CARMA CO (1–0) data (top spectra in each panel) with other molecular tracers, uncluding a JCMT single-dish HCO^+ (3–2) observation of V806 Tau, a JCMT CO (3–2) observation of V892 Tau, and a CSO CO (6–5) observation of V892 Tau (Chapter 2, Salter et al. 2010a; Thi et al. 2001).

Clearly, the 1.3 mm continuum fluxes, which probe the cold dust reservoir at all radii, are a poor predictor of the integrated line strengths in this sample.

The other mid-infrared dust diagnostics (e.g. grain growth and dust settling) also offer few properties aligned with our detection statistics. Both sources with large amounts of dust settling (DQ Tau) and small amounts (V806 Tau) can present similarly bright and resolved CO emission lines ($\sim$40 mJy bm^{-1}); the results are identical for an abundance of small grains (V806 Tau and V892 Tau) versus a more depleted population (DQ Tau) in the disk surface layers. Therefore, the mid-infrared dust properties probing the warm inner regions also appear to be poor indicators of the relative CO line strength in this sample.

We can also compare the dust diagnostics with the gas-line properties for the entire literature for sources in Taurus with $F_{1.3\mathrm{mm}} \geq 75$ mJy, to look for larger observational trends. However, similar examples of contrasting dust and gas observational diagnostics are also present in the larger sample. For example, DN Tau, DM Tau, and GM Aur all exhibit an equally bright 3–2 line, as measured by Andrews (2007), and yet their 1.3 mm continuum fluxes range 84–253 mJy. In addition, DN Tau is not detected in 1–0 or 2–1 (Schaefer et al. 2009), in contrast to the other two sources (Koerner et al. 1993a; Dutrey et al. 1997; Panić et al. 2008; Simon et al. 2000; Kessler-Silacci 2004). CY Tau, DL Tau, and DO Tau are all detected (one faintly, another strongly) in the 2–1 transition (Simon et al. 2000; Koerner & Sargent 1995); and they all possess a depleted small-grain population ($S_{10\mu\mathrm{m}} = 0.09$–$0.18$). In contrast, DM Tau, GM Aur, and RY Tau exhibit more small-grain emission ($S_{10\mu\mathrm{m}} = 0.96$–$1.36$) and are also strongly detected (Koerner et al. 1993a).

In the Dutrey et al. (1996) survey of ^{13}CO, an optically thinner isotope of ^{12}CO, the authors find disk masses predicted from the dust emission were 20–80 times larger than the masses derived from the ^{13}CO of 3 detected sources (DG Tau, Haro 6-5b, and UY Aur), suggesting that the lines toward these sources may not trace the entire gas reservoir. Many explanations can account for this discrepancy, including CO freeze-out onto dust grains in the cold regions of the disk, preferential dispersal of the gas content in disks, or optically thick intervening material. In the case of DG Tau, one of the brightest sources in the continuum in Taurus, several follow-up interferometric studies confirm a highly confused circumstellar

environment that significantly obscures the line emission (Kitamura et al. 1996; Testi et al. 2002).

In fact, confusion by foreground material is a common thread in the literature (as well as our own source sample), and particularly apparent in interferometry data where the maximum obscuration of the line typically occurs near the systematic velocity of the cloud (and the star itself). Other confirmed examples of strongly afflicted sources include DL Tau and UZ Tau E (Simon et al. 2000), and V806 Tau and GO Tau (Schaefer et al. 2009). Fewer examples exist of sources that are well isolated, like DM Tau and GM Aur (Dutrey et al. 1998; Simon et al. 2000; Panić et al. 2008). Identifying more *isolated*, gas-rich sources or probing optically thinner molecular species or higher transitions is necessary to achieve a uniform, less contaminated analysis of the observational diagnostics for the gas reservoir.

3.6 Summary

We observed 5 classical T Tauri stars (CW Tau, DQ Tau, IQ Tau, V806 Tau, and V892 Tau) in low-J transitions of ^{12}CO to contrast the observed gas properties in a sample of disks in different dust evolutionary stages. These observations complete the interferometric sampling of at least one CO rotational line toward the brightest 1.3 mm sources ($F_{1.3\mathrm{mm}} \geq 75$ mJy) in the Taurus star-forming region. Here we report 2 new detections of a CO (1–0) line and 1 detection of CO (2–1) to be added to the growing literature of molecular line observations of the protoplanetary disks around T Tauri stars; which are characterized by a low statistical detection rate overall for low-J CO line observations.

Using the CARMA millimeter array, we measured 2.7 mm continuum fluxes for all sources, resolving just the brightest two sources, V806 Tau and V892 Tau. These are also the only two sources to be detected in CO (1–0). The CO emission around V806 Tau is resolved and appears clumpy in nature; V892 Tau is unresolved. In both CO integrated spectra, several peaks are seen spread out over large velocity separations (of full breadth 6–12 km s^{-1}) and still appear to be associated with the source position. Their radial location in the map is consistent with the disk extent and the radial velocity offsets for the peaks are consistent with Keplerian rotational velocities at radii $\lesssim 30$ AU. The surrounding sky regions in the maps of all 5 sources are dotted with 2–3σ emission peaks, suggesting that a lot of CO may be present in the region. This conclusion is supported by the visibility data sets of CW Tau and V892 Tau, in particular, which show that additional CO emission is detected on the shortest baselines only, representing larger-scale structure in the field. When comparing our interferometry data to single-dish observations and other interferometry results in the literature, our CO spectra clearly suffer from obscuration, which is a common trend in studies of the gas structure and kinematics toward sources in crowded, star-forming regions.

In supplementary observations of DQ Tau obtained with the SMA, we report an unresolved 1.3 mm continuum flux measurement and a strong CO (2–1) emission line that *is* resolved. From a Gaussian fit to the visibility data, the gas component extends to a radius three times larger than the dust and has an inclination angle (62°) that differs from the dust disk (62°). It is interesting how DQ Tau, which until now has remained undetected in rotational lines of several molecular tracers, appears as a bright line in this transition. Sensitivity levels may be partly to blame. However, the thin, sharp, double-peak nature of our low spectrally resolved 2–1 line profile is more indicative of absorption effects along the line-of-sight rather than a purely Keplerian disk velocity pattern. Therefore, we suspect that intervening cloud material could likely play a role in the non-detected lines toward this source. This result iterates the unpredictable nature of the observed gas-line intensities, especially if we try to extrapolate directly from the observed dust measurements.

When considering the entire literature sample, we found no significant trends in the CO line intensity or detection statistics with any of the current diagnostics for the dust evolutionary state (e.g. dust mass, grain growth, and dust settling properties). In addition, two sources that are equally bright in one CO

transition line do not necessarily possess similar brightnesses in another transition. Almost all sources exhibit some level of obscuration from optically thick CO along the line-of-sight, accounting for some of these observational differences.

Our primary conclusion from this study is that enough CO is confirmed present along the line-of-sight toward 4/5 of our targets (CW Tau, DQ Tau, V806 Tau, and V892 Tau) to be optically-thick in the low-*J* transitions, prohibiting an accurate study of the gas distribution and disk kinematics based on these diagnostics alone, even with interferometers and increased sensitivity observations. We therefore caution that low-*J* CO lines are likely a poor tracer of the total disk gas content and that they may not be accurate predictors of the line strengths of mid-*J* transitions that offer greater contrast with the cloud material. The low-*J* data can only provide constraints, and better characterization of the environment is necessary to determine the robustness of these constraints.

Acknowledgements

Support for CARMA construction was derived from the states of California, Illinois, and Maryland, the Gordon and Betty Moore Foundation, the Kenneth T. and Eileen L. Norris Foundation, the Associates of the California Institute of Technology, and the National Science Foundation. Ongoing CARMA development and operations are supported by the National Science Foundation under a cooperative agreement, and by the CARMA partner universities. The research of DMS and MRH is supported through a VIDI grant from the Netherlands Organization for Scientific Research (NWO).

Bibliography

Andrews, S. M. 2007, PhD thesis, University of Hawai'i at Manoa
Basri, G., Johns-Krull, C. M., & Mathieu, R. D. 1997, AJ, 114, 781
Beckwith, S. V. W., Sargent, A. I., Chini, R. S., & Guesten, R. 1990, AJ, 99, 924
Boden, A. F., Akeson, R. L., Sargent, A. I., et al. 2009, ApJ, 696, L111
Calvet, N., D'Alessio, P., Hartmann, L., et al. 2002, ApJ, 568, 1008
Dullemond, C. P., van Zadelhoff, G. J., & Natta, A. 2002, A&A, 389, 464
Dutrey, A., Guilloteau, S., Duvert, G., et al. 1996, A&A, 309, 493
Dutrey, A., Guilloteau, S., & Guelin, M. 1997, A&A, 317, L55
Dutrey, A., Guilloteau, S., Prato, L., et al. 1998, A&A, 338, L63
Fedele, D., van den Ancker, M. E., Acke, B., et al. 2008, A&A, 491, 809
Furlan, E., Hartmann, L., Calvet, N., et al. 2006, ApJS, 165, 568
Guilloteau, S. & Dutrey, A. 1998, A&A, 339, 467
Hamidouche, M. 2010, ArXiv e-prints
Ida, S. & Lin, D. N. C. 2004, ApJ, 616, 567
Johansen, A., Youdin, A., & Mac Low, M. 2009, ApJ, 704, L75
Jørgensen, J. K., Schöier, F. L., & van Dishoeck, E. F. 2004, A&A, 416, 603
Kenyon, S. J., Dobrzycka, D., & Hartmann, L. 1994, AJ, 108, 1872
Kessler-Silacci, J. 2004, PhD thesis, CALIFORNIA INSTITUTE OF TECHNOLOGY
Kessler-Silacci, J., Augereau, J., Dullemond, C. P., et al. 2006, ApJ, 639, 275
Kitamura, Y., Kawabe, R., & Saito, M. 1996, ApJ, 457, 277
Koerner, D. W. & Sargent, A. I. 1995, AJ, 109, 2138
Koerner, D. W., Sargent, A. I., & Beckwith, S. V. W. 1993a, Icarus, 106, 2
Koerner, D. W., Sargent, A. I., & Beckwith, S. V. W. 1993b, ApJ, 408, L93
Mathieu, R. D., Stassun, K., Basri, G., et al. 1997, AJ, 113, 1841

Monnier, J. D., Tannirkulam, A., Tuthill, P. G., et al. 2008, ApJ, 681, L97
Moriarty-Schieven, G. H., Wannier, P. G., Tamura, M., & Keene, J. 1992, ApJ, 400, 260
Öberg, K. I., Qi, C., Fogel, J. K. J., et al. 2010, ApJ, 720, 480
Panić, O. & Hogerheijde, M. R. 2009, A&A, 508, 707
Panić, O., Hogerheijde, M. R., Wilner, D., & Qi, C. 2008, A&A, 491, 219
Panić, O., Hogerheijde, M. R., Wilner, D., & Qi, C. 2009, A&A, 501, 269
Salter, D. M., Hogerheijde, M. R., & Blake, G. A. 2008, A&A, 492, L21
Salter, D. M., Hogerheijde, M. R., van der Burg, R. F. J., Kristensen, L. E., & Brinch, C. 2010a, A&A submitted
Salter, D. M., Kóspál, Á., Getman, K. V., et al. 2010b, ArXiv e-prints
Schaefer, G. H., Dutrey, A., Guilloteau, S., Simon, M., & White, R. J. 2009, ApJ, 701, 698
Schreyer, K., Guilloteau, S., Semenov, D., et al. 2008, A&A, 491, 821
Simon, M., Dutrey, A., & Guilloteau, S. 2000, ApJ, 545, 1034
Testi, L., Bacciotti, F., Sargent, A. I., Ray, T. P., & Eislöffel, J. 2002, A&A, 394, L31
Thi, W. F., van Dishoeck, E. F., Blake, G. A., et al. 2001, ApJ, 561, 1074
van Kempen, T. A., van Dishoeck, E. F., Brinch, C., & Hogerheijde, M. R. 2007, A&A, 461, 983